PERGAMON

Micron 32 (2001) 341–353

micron

www.elsevier.com/locate/micron

A study of fibrous long spacing collagen ultrastructure and assembly by atomic force microscopy ☆

M.F. Paige, J.K. Rainey, M.C. Goh*

Department of Chemistry, University of Toronto, Toronto, Ontario, Canada M5S 3H6

Abstract

Fibrous long spacing collagen (FLS) fibrils are collagen fibrils that display a banding with periodicity greater than the 67 nm periodicity of native collagen. FLS fibrils can be formed in vitro by addition of α_1-acid glycoprotein to an acidified solution of monomeric collagen, followed by dialysis of the resulting mixture. We have investigated the ultrastructure of FLS fibrils formed in vitro using the atomic force microscope (AFM). The majority of the fibrils imaged showed typical diameters of ~150 nm and had a distinct banding pattern with a ~250 nm periodicity. However, we have also observed an additional type of FLS fibril, which is characterized by a secondary banding pattern surrounding the primary bands. These results are compared with those obtained in past investigations of FLS ultrastructure carried out using the transmission electron microscope (TEM). The importance of the fibril's surface topography in TEM staining patterns is discussed. Images of FLS fibrils in various stages of assembly have also been collected, and the implications of these images in determining the mechanism of assembly and the formation of the characteristic banding pattern of the fibrils is discussed.

Keywords: Collagen; Atomic force microscopy; Fibrous long spacing collagen; Assembly; Ultrastructure; Transmission electron microscopy; Negative staining

1. Introduction

1.1. Fibrous long spacing collagen

Type I collagen fibrils in their native form typically display a banding pattern with 67 nm spacing when visualized with electron microscopy (EM) (Ghadially, 1988; Nimni, 1988) or atomic force microscopy (Baselt et al., 1993; Revenko et al., 1994). Collagen, however, is a system which shows a large degree of polymorphism. Depending upon the in vivo or in vitro conditions of assembly, collagen molecules may form a variety of different structures. One important variation of the fibrous forms of Type I collagen are those classified as "fibrous long spacing" collagen fibrils (FLS). By definition, any collagen fibril with a periodicity greater than 67 nm can be considered as FLS collagen (Ghadially, 1988).

The first observation of FLS type collagen was made in 1950 by Highberger et al. during the examination of fibrous structures formed by the dialysis of an acidified connective tissue extract (Highberger et al., 1950). The fibrils produced by dialysis displayed a banding periodicity of ~200–300 nm in the transmission electron microscope (TEM). Because the collagen monomer is ~280 nm in length (Nimni, 1988), this observation led to the hypothesis that FLS collagen was formed by collagen monomers lined up in register, taking on a random head-to-tail, head-to-head or tail-to-tail alignment (Fig. 1) (Gross et al., 1954). Despite its preliminary nature, this has essentially become the accepted model for FLS collagen structure (Chapman and Armitage, 1972; Franzblau et al., 1976; Ghadially, 1988).

During subsequent investigations by Highberger et al., it was found that careful purification of collagen solutions inhibited the formation of FLS fibrils. This suggested that a second component, removed by the more careful purification scheme, was necessary for inducing FLS formation. Further work suggested this component was α_1-acid glycoprotein (Highberger et al., 1951), a species commonly found in mammalian plasma. A comparison of FLS and native collagen fibril amino acid compositions using radioactively labelled α_1-acid glycoprotein suggested that α_1-acid glycoprotein is incorporated directly into the FLS fibrils (Franzblau et al., 1976). However, the exact roles of the α_1-acid glycoprotein in both fibril formation and morphology have yet to be determined.

☆ Supported by grants from the American Chemical Society Petroleum Research Fund, the Natural Science and Engineering Research Council of Canada, and Photonics Research Ontario.

* Corresponding author. Tel.: +1-416-978-6254; fax: +1-416-978-6254.
E-mail address: cgoh@chem.utoronto.ca (M.C. Goh).

0968-4328/00/$ - see front matter
PII: S0968-4328(00)00037-8

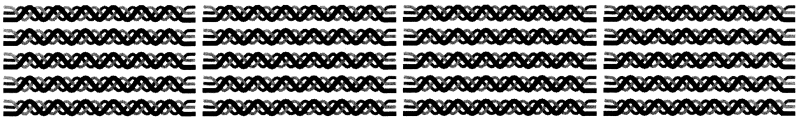

Fig. 1. Hypothesized structure (Gross et al., 1954) of in vitro FLS collagen fibril with schematic representation of collagen monomers (~280 nm in length). The observed periodicity in electron micrographs of FLS collagen (Highberger et al., 1950, 1951; Gross et al., 1954) is accredited to the spacing between rows of monomers. Note that no directionality is implied for the monomers.

Polysaccharides such as chondroitin sulphate and heparin sulphate have also been reported to form FLS collagen fibrils during reconstitution (Gross et al., 1952; Chapman and Armitage, 1972). However, it should be noted that Lowther et al. (1970) were unable to form FLS collagen with such polysaccharides. This variation on the FLS collagen fibrillogenesis system is currently under investigation in our laboratory.

Soon after the first in vitro detection of FLS collagen, Jakus (1956) detected it in vivo in ocular tissue. FLS collagen has since been detected in a variety of normal and pathological tissues (Ghadially, 1988). Characteristic occurrences have been in nervous tissue, with early observations in both normal (Cauna and Ross, 1960) and cancerous tissue (Luse, 1960; Naumann and Wolfe, 1963). Other pathological situations in which FLS collagen has been observed are atherosclerotic plaques (Morris et al., 1978), Hodgkin's disease (Nakanishi et al., 1981), myeloproliferative disorder (Kamiyama and Shimamine, 1977; Kamiyama, 1982) and silicosis (Slavin et al., 1985).

Interestingly, the banding periodicity that is most frequently observed in vivo is approximately half that of FLS collagen formed in vitro (~100–150 nm as compared with ~200–300 nm (Ghadially, 1988)). This has lead to the hypothesis that FLS collagen formed in vivo is simply made up of collagen monomers aligned in a half-stagger. In one case, however, FLS collagen from a heomorrhagic and necrotic tissue specimen was observed to have a banding periodicity of ~250 nm (Ghadially and Mierau, 1985). The general discrepancy in banding between the in vitro and in vivo FLS fibrils is puzzling, because studies have shown that FLS collagen formed in vivo also contains glycoproteins (Ghadially, 1988; Dingemans and Teeling, 1994). Under the correct conditions, native-type collagen fibrils (67 nm periodicity) formed in vitro may have highly similar, if not identical, morphologies to those formed in vivo (Williams et al., 1978); this appears not to be the case for FLS fibrils.

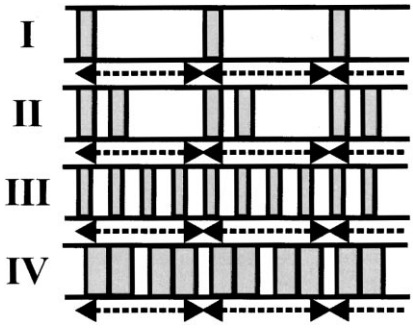

Fig. 2. Schematic representation of the four proposed morphologies of in vitro FLS collagen fibrils classified by transmission electron microscope analysis (Chapman and Armitage, 1972). The dashed arrow represents one period of an FLS collagen monomer (i.e. ~230–260 nm).

Given that FLS collagen formed in vivo has been shown to contain glycoproteins, the most fundamental hypothesis for FLS collagen formation is that glycoproteins or polysaccharides are directly involved, as appears to be the case in vitro (Hashimoto and Ohyama, 1974; Ghadially, 1988; Dingemans and Teeling, 1994). However, this does not explain why FLS fibrils in vivo are occasionally formed instead of native collagen.

Currently, there are two hypotheses accounting for the driving force for formation of FLS fibrils in vivo. In the first, proposed by Kajikawa et al. (1980), the degradation of reticular collagen by collagenase is proposed to play an important role. This was shown by the promotion and inhibition of collagenase activity in tissue cell culture, with a large amount of FLS collagen being produced upon elevation of collagenase activity. In the case of EDTA inhibition of collagenase, no FLS collagen was observed. Upon introduction of bacterial collagenase to the treated culture, however, FLS collagen was again produced. An independent study by Kobayasi et al. (1985) confirmed increased FLS formation promoted by collagenase activity. In the second proposed mechanism, from Park and Ohno (1985), glycosaminoglycans from basal laminae of neoplastic cells are thought to interact with immature collagen fibrils and promote FLS collagen formation. This was postulated after histochemical examination of neural tumors, in which FLS collagen appeared to be contiguous with the basal laminae. Additional studies from the same research group showed further cases in which FLS collagen was associated with basal laminae (Miki et al., 1993). Of course, it is possible that FLS collagen in vivo may be formed through either mechanism, depending upon the physiological conditions in a given tissue. It is also quite possible that there are other, as of yet undetermined, mechanisms of in vivo FLS collagen formation.

It is worth noting that FLS collagen formed in vitro can exhibit polymorphism, even within the same fibril. As depicted schematically in Fig. 2, Chapman and Armitage (1972) classified FLS collagen into four different categories—Types I–IV—depending upon the banding pattern observed in the TEM. Based upon the observed patterns, various monomer stagger patterns were proposed for the

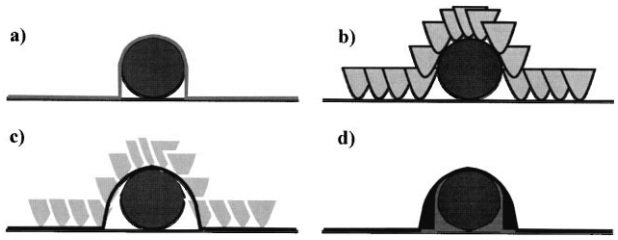

Fig. 3. Schematic illustration of tip convolution effect. If a rounded object were imaged with an ideal, atomic sized AFM tip, the trace shown in (a) would result. The actual convoluted image produced by the path of the grey, realistically shaped tip in (b) is shown by the trace in (c). In (d), the additional area produced by the tip convolution is shaded darkly. The inaccessible inwardly curving area beneath the widest point of the sample, even with an ideal (or de-convoluted) image, means that the more lightly shaded area in (d) can never be imaged by the AFM.

structures of each of the types I–IV FLS collagen. In the following sections, we will discuss some of our attempts to correlate atomic force microscope (AFM) images of FLS collagen with the types of FLS collagen proposed by Chapman and Armitage.

As noted, the previous models for FLS collagen structure have been based upon stagger patterns of collagen monomers in the fibril body (Gross et al., 1954; Chapman and Armitage, 1972). However, these models have been difficult to reconcile with the fibrillar ultrastructure which we have previously observed by AFM (Paige et al., 1998). Therefore, we will compare the FLS collagen morphologies observed by AFM with those seen by Chapman and Armitage, but will not extend the comparison to their proposed monomer stagger models.

1.2. Atomic force microscopy

In general, both the structure and formation mechanism (fibrillogenesis) of FLS collagen remains poorly characterized. We have attempted to provide insight into both of these important topics through the application of the atomic force microscopy (AFM).

Despite its moderately recent invention by Binnig et al. (1986), the AFM has rapidly become a widely used technique for characterising surface properties of biological macromolecules (for recent reviews see Shao and Zhang, 1996; Bustamante et al., 1997; Hansma et al., 1997). While more complicated variations of the technique have been developed, the basic principle of the AFM is that a sharpened probe tip attached to a flexible cantilever arm is scanned across a surface of interest. Interactions between the tip and sample are used to map out various properties of the surface, the most commonly measured being topography.

In its simplest mode of operation, often referred to as ‘contact mode’ imaging, the AFM tip is brought directly into contact with the surface of interest and raster scanned. The deflection of the cantilever upon which the tip is mounted is monitored and used as a feedback mechanism to control the interaction between tip and sample. By maintaining a constant cantilever deflection throughout the scanning process, one can generate highly accurate topographical measurements of the surface. Images produced in this way are usually referred to as height images. Modern commercial instruments boast vertical resolution on the order of ∼0.01 nm and lateral resolution of around 0.1–3 nm (Sarid, 1991).

When large changes in sample topography are encountered, the feedback loop employed to keep the cantilever deflection constant may not be able to respond rapidly enough, producing an error in the height signal. This error signal may be used as an additional source of contrast, producing a so-called “deflection image”. Deflection images are often useful, because increased contrast occurs at the edges of objects, highlighting features which may not be easily distinguished in the height image. It must be emphasized, however, that deflection images are only used as an aid in feature visualization, and that all quantitative analyses need be performed on the topographic “height image”.

An important consideration when imaging with the AFM is the so-called “convolution effect”, which is introduced because of the finite width of the probe tip. The digital images produced by the AFM are a combination of both the topography of the sample and that of the probe tip. The basic principles of tip convolution are illustrated in Fig. 3. An ideal AFM tip would be atomic in size, and when scanned across a sample, would faithfully reproduce all surface features. Such an ideal trace is shown in Fig. 3a. As is apparent in Fig. 3a, features below the lateral apex of an object cannot be resolved. This fact must be kept in mind during AFM image analysis. A real AFM tip has a finite size and shape, which may differ from tip to tip, even for tips from the same manufacturer. As a real AFM tip passes over a sample (e.g. Fig. 3b), its shape will contribute to the image as shown by the trace in Fig. 3c. This leads to a general widening of features, an effect referred to as convolution (Chicon et al., 1987; Keller, 1991). The illustration in Fig. 3d shows regions of the sample which can not be imaged because of their inaccessibility to the AFM tip and because of tip–sample convolution.

While tip convolution effects are present in all AFM images, their significance depends upon the size of the features being imaged. For surface features that are large in comparison with the size of the AFM tip (∼tens of nanometers), convolution effects tend to be minimal. However, if features have sizes which are comparable with the tip, then particular care must be taken to account for this effect when taking measurements from the image. One method of dealing with tip convolution is to use processing software to subtract the shape of the tip from the image (Keller, 1991; Markiewicz and Goh, 1994). However, these techniques generally require prior knowledge of the tip shape to be truly effective. While one can characterize the tip geometry before every experiment, either by using

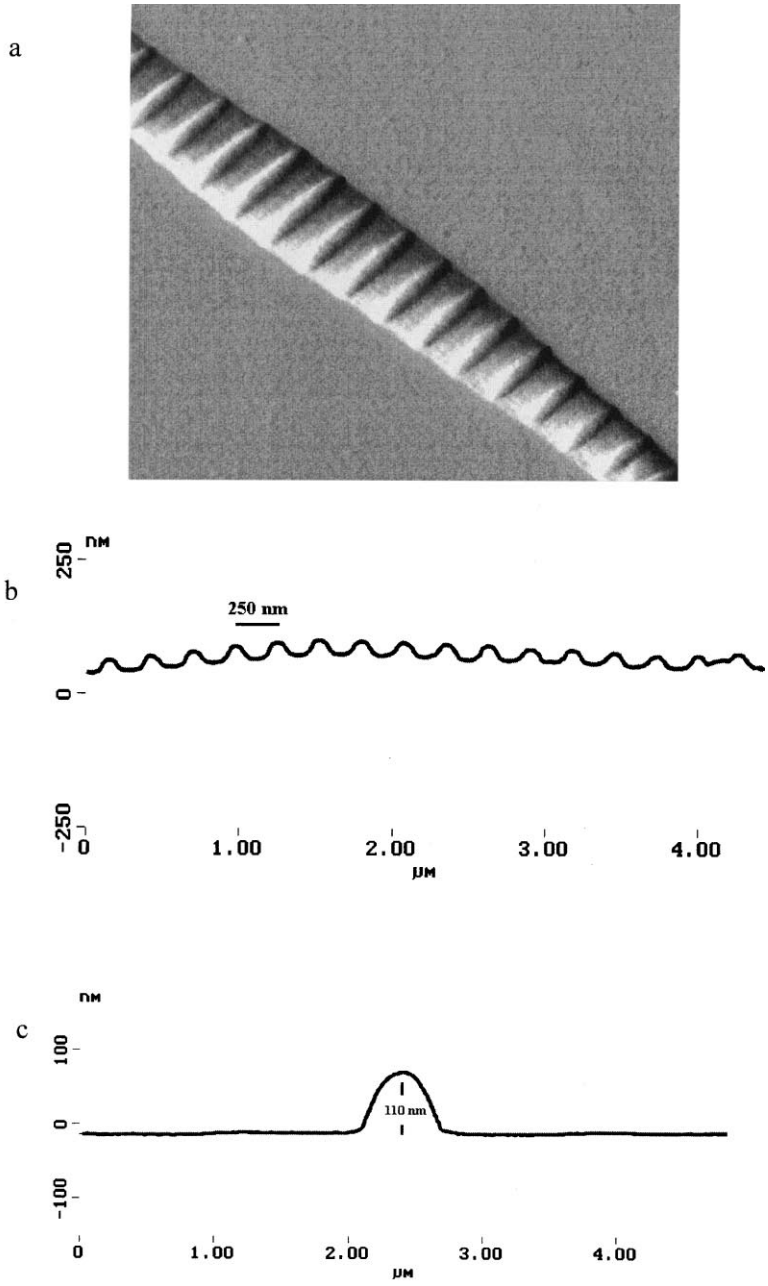

Fig. 4. AFM images and sectional analyses of FLS and native collagen fibrils; (a) Deflection mode image of FLS collagen fibril ($3.5 \times 3.5\ \mu m^2$); (b) longitudinal section of FLS collagen fibril; note ~250 nm periodicity; (c) cross-section of FLS collagen fibril; (d) deflection mode image of native collagen fibril ($2.5 \times 2.5\ \mu m^2$); (e) longitudinal section of native collagen fibril; (f) cross-section of native collagen fibril.

electron microscopy or by using calibration standards in the AFM (Markiewicz and Goh, 1994), doing so would be very time consuming. Furthermore, the tip shape may change during the course of imaging because of adhesion of fragments from the sample, rendering the tip shape data inaccurate. Precise imaging of nanometer scale features merits this kind of rigorous and time consuming treatment. Generally, however, these deconvolution approaches are not used in a routine manner. Through prudent analysis of data and repeated imaging of the same sample with different tips, routine imaging can be performed without the need for deconvolution routines.

2. Materials and methods

2.1. In vitro FLS collagen assembly

Type I calf-skin collagen (~95% purity, Sigma, St. Louis, MO) was dissolved over ice in 0.05% acetic acid,

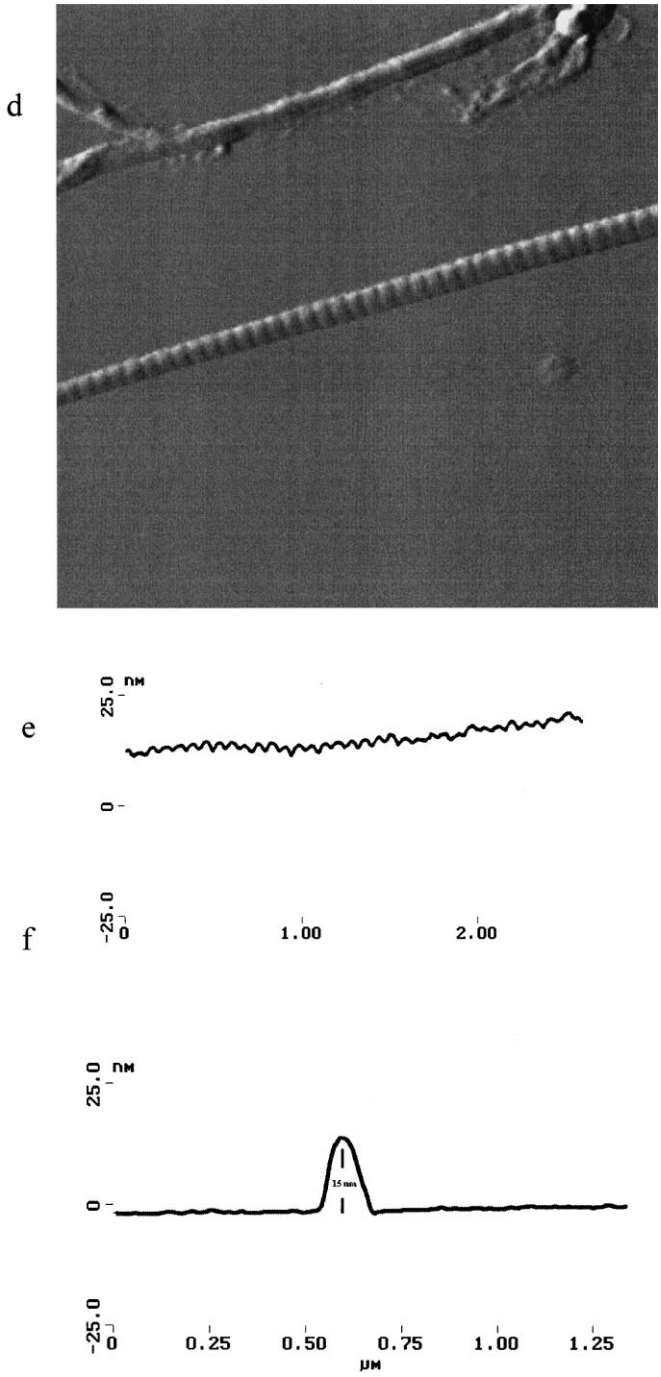

Fig. 4. (*continued*)

with occasional sonication to facilitate the breakdown of collagen aggregates. The mixture was centrifuged at 10 000 rpm for 60 min at 4°C. After centrifugation, the supernatant was filtered through 0.45 μm Millipore filters (Sigma) and mixed with the α_1-acid glycoprotein solution. Solutions of various α_1-acid glycoprotein concentrations were prepared by dissolving the solid bovine serum derived protein (99% purity, Sigma) in 0.05% acetic acid (v/v). Collagen and glycoprotein solutions were combined to yield a mixture with a final collagen concentration of ~0.5 mg/ml, an α_1-acid glycoprotein concentration ranging from 0 to 0.75 mg/ml and a final pH of 3.5. The protein mixture was transferred into dialysis tubing (molecular weight cutoff 12–14 kDa) and dialysed at 21°C against Millipore filtered water overnight (~17 h). Dialysis produced a white, turbid solution with a final pH of 7. A series of dilutions ranging from 10- to 1000-fold were prepared by mixing the dialysis product with an appropriate volume of Millipore water. The diluted samples were deposited onto freshly cleaved sheets of mica in 20 μl aliquots

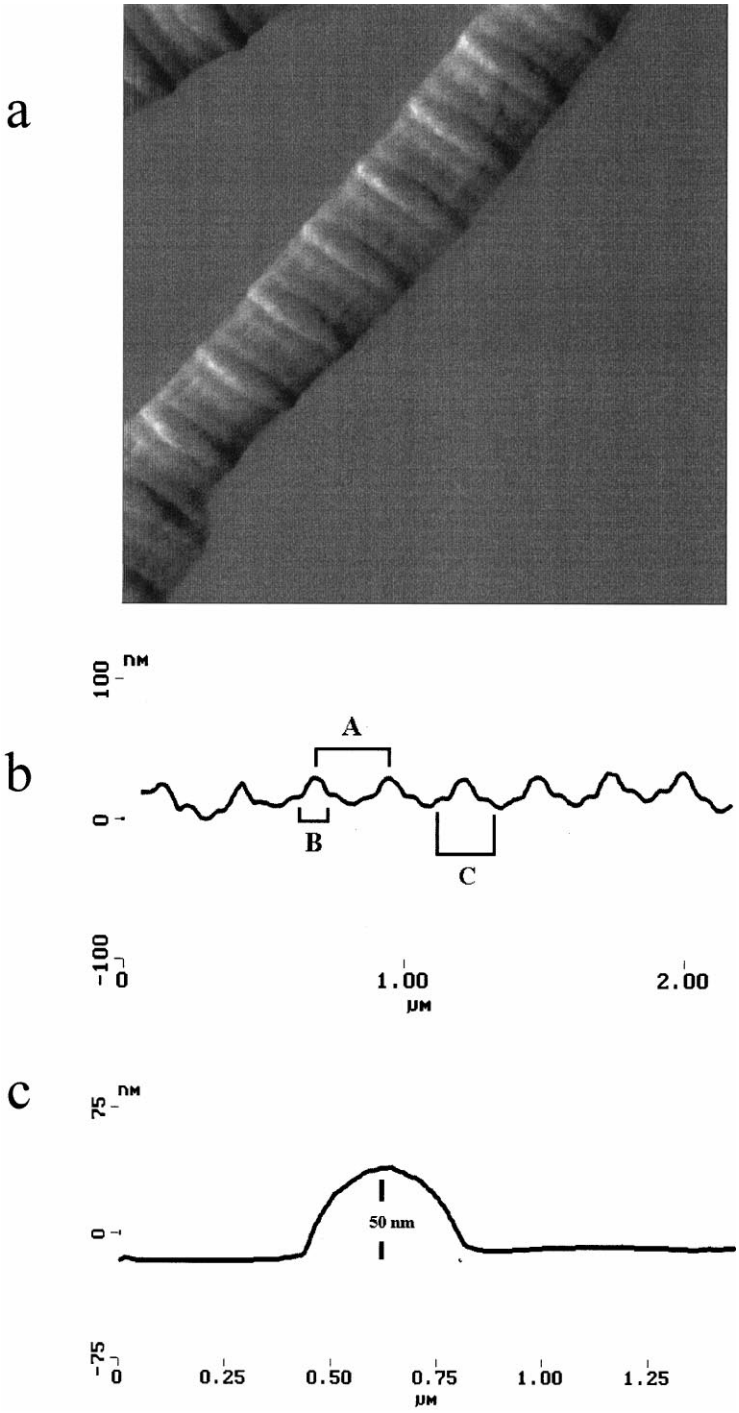

Fig. 5. AFM image and sectional analyses of new FLS collagen variant; (a) deflection mode image of FLS collagen variant ($2 \times 2\ \mu m^2$); (b) longitudinal section of FLS collagen variant; (c) cross-section of FLS collagen variant.

and dried, either under a stream of filtered nitrogen or at ambient temperature and pressure under air, prior to imaging with the AFM.

2.2. Atomic force microscopy

Samples were imaged with a Nanoscope III instrument (Digital Instruments, Santa Barbara, CA), typically using square pyramidal silicon nitride tips of spring constant 0.58 N/m. Occasionally, oxide-sharpened tips were used for imaging. Images were obtained using contact mode in air. Electron microscopy locator grids were fixed underneath the mica prior to cleavage in order to facilitate the repeated examination of the same area of a given sample (Markiewicz and Goh, 1997). Tips were changed frequently in order to check for possible tip artefacts. Both height and

Table 1

Collagen fibril type	Native	"Type A" FLS	"Type B" FLS
Typical diameter	~10–30 μm	~100–200 nm	~50 nm
Typical length	Tens of μm	Tens of μm	Tens of μm
Banding periodicity	~67 nm	~250 nm	~250 nm
Band nature	Bumps with no discernable flat interband region	Protrusions separated by flat interband regions	Peaks surrounded by ridges; separated by flat interband regions
Band height above interband region	Order of nm	~25–30 nm	Ridges: ~6 nm Peaks: ~18 nm
Band width	Full period (~67 nm)	~90–100 nm	Ridges: ~70–90 nm Peaks: ~90–100 nm

defelction mode images were taken simultaneously, with height measurements being taken from the height mode images only.

3. Results and discussion

3.1. Native-type versus FLS collagen ultrastructure

The majority of the FLS fibrils imaged have ultrastructural properties that are indistinguishable from those we have reported previously (Paige et al., 1998). A typical fibril, along with its lateral and longitudinal cross-sections, is shown in Fig. 4a–c. For sake of comparison, we have included similar images and sections of a native-type fibril, shown in Fig. 4d–f. FLS fibrils are typically ~100–200 nm in diameter and tens of microns in length, with accurate measurements of the latter dimension being hampered by the entangled nature of the fibrils. The fibrils are highly periodic, with a banding pattern of ~250 nm. Native-type fibrils formed in vitro are typically much thinner, having diameters in the range of 10–30 nm. Their periodicities are ~67 nm and they have lengths, which are comparable with those of FLS.

As is apparent in Fig. 4b, the banding pattern of FLS is caused by a series of evenly spaced protrusions, separated by long, moderately flat interband regions. These protrusions are typically of the order of ~25–30 nm higher than the interband regions and have a width of ~100 nm. This is in contrast to the native-type fibrils, in which the bands are caused by a continuous series of bumps, as shown in Fig. 4e. For FLS, the distance between bands is large enough that the AFM tip can be used to probe the underlying ultrastructure. Examination of the interband and band regions reveals a series of grooves which run parallel to the main axis of the fibrils. These grooves appear to be continuous through both the band and interband regions. The depths of the grooves are on the order of 2 nm, with widths of ~20–25 nm.

The ability to resolve the depth and width of the grooves is limited by the finite size of the AFM tip; the measured depths will be underestimates because of the inability of the tip to penetrate into regions which are narrower than itself, while convolution effects will make the measured widths appear somewhat larger than they actually are. We have previously ascribed these grooves to be caused by spaces between tightly packed protofibrils, which appear to be stable intermediates in the growth of the mature fibril. This topic shall be explored in greater detail in a later section.

3.2. Novel FLS fibril ultrastructure

As stated, the majority of FLS fibrils observed showed the characteristic features described above. For sake of convenience, fibrils with the previously described ultrastructure shall temporarily be referred to as 'Type A' fibrils. Occasionally, fibrils with an ultrastructure, which is different from Type A are observed, as shown along with appropriate cross-sections in Fig. 5a–c. The second type of FLS fibril, which we shall refer to as 'Type B', again possesses a series of periodic bands running along the length of the fibril at ~250 nm periodicity (A in Fig. 5a). In Type B collagen, however, each band consists of two minor ridges surrounding a larger, central peak. A narrow interband region separates adjacent bands. The central peak is typically of the order of ~18 nm above the lowest point on the interband region, while the smaller ridges are ~6 nm high. The width of the central peak, labeled as B in Fig. 5a, is ~80–100 nm, while the width of the minor ridges are ~70–90 nm. The entire band has a width of ~220 nm (C in Fig. 5a). Diameters of the Type B fibrils are generally smaller than Type A, being typically around 50 nm, while their lengths are, again, on the order of tens of microns. The main features of Types A and B FLS and of native collagen fibrils are summarized in Table 1.

We have explored a range of α_1-acid glycoprotein concentrations to see if this parameter plays any apparent role in the formation of one FLS polymorph over another. Over the range of α_1-acid glycoprotein concentrations explored, we saw no particular tendency to form one variant of FLS over another. However, we did observe that at total glycoprotein concentrations between 0.1 and 0.2 mg/ml, a mixture of native-type (~67 nm periodicity) fibrils and FLS

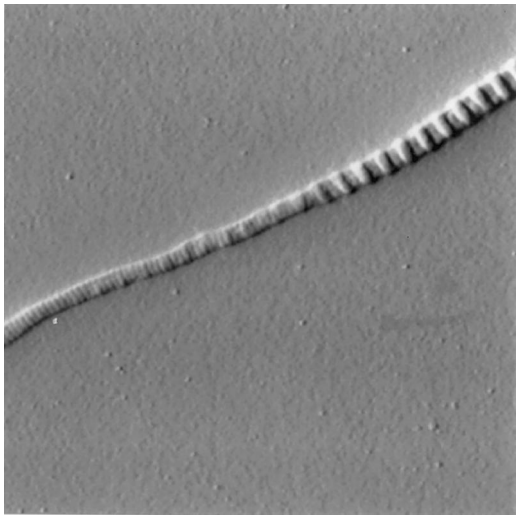

Fig. 6. Deflection mode image of hybrid FLS/native collagen fibril. Periodicity on the left-hand side of the fibril is the ~67 nm of native collagen, while that on the right is the ~250 nm of FLS ($10 \times 10\ \mu m^2$).

fibrils are formed. One occasionally observes hybrid fibrils, showing both FLS and native-type periodicity on the same fibril (Fig. 6). Above this glycoprotein concentration range, FLS only is observed; below, only native-type is observed. Unlike Franzblau et al. (1976), who observed the complete inhibition of fibril formation at very high collagen to glycoprotein ratios, we observed the formation of native-type fibrils at all glycoprotein concentrations below 0.1 mg/ml. The most obvious explanation for this is that the glycoprotein is incorporated directly into the growing fibril. If the glycoprotein is not present in sufficient quantity, the fibril assembly 'defaults' into forming native fibrils. Presumably, at concentrations in the range of 0.1–0.2 mg/ml, there are regions in the reaction mixture, which contain sufficiently high local concentrations of glycoprotein to promote FLS formation.

We have carried out experiments with fluorescently labeled glycoprotein and, using fluorescence spectroscopy and confocal microscopy, attempted to determine its role in the assembly. Preliminary experiments indicate that glycoproteins are incorporated directly into the FLS fibrils, confirming those by Franzblau et al. (1976). However, we have not yet been able to obtain the spatial resolution required to pinpoint their exact location (e.g. in the bands, interband region etc.). With the recent development of near-field scanning optical microscopy (NSOM) (Dürig et al., 1986; for recent reviews see Meixner and Kneppe, 1998; Lewis et al., 1999; Shiku and Dunn, 1999), the required resolution might now be attained to answer this fundamental question.

3.3. Comparison of fibril banding patterns observed by AFM and TEM

The transmission electron microscopy (TEM) has

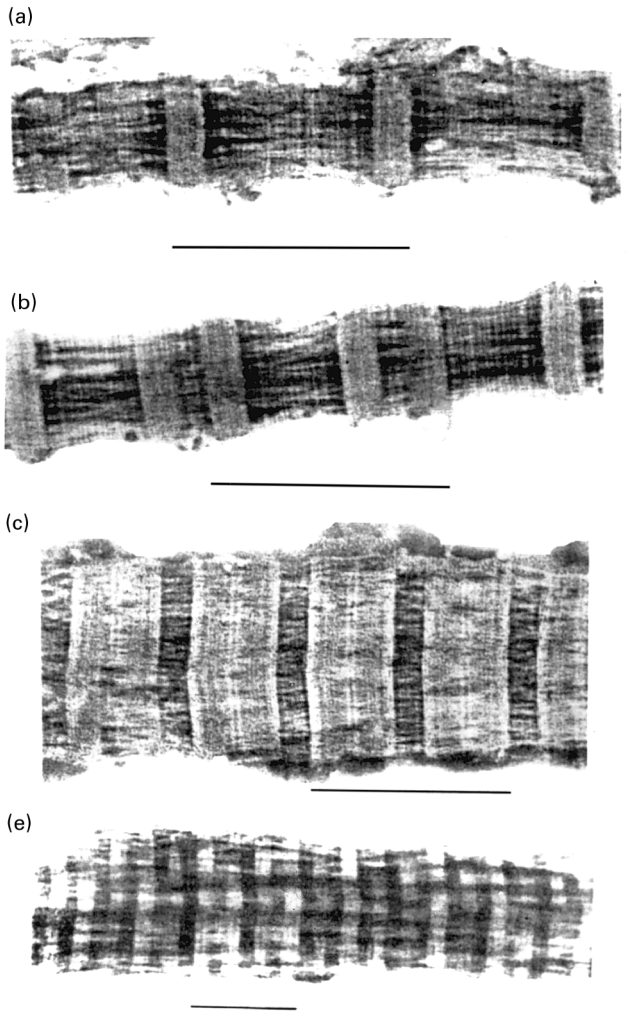

Fig. 7. TEM micrographs of FLS collagen variants reproduced from Chapman and Armitage (1972) with permission of the publisher. The scale in these images is indicted by the solid line, which represents the approximate length of an individual collagen monomer. (a) FLS I (one narrow overlap band per monomer length); (b) FLS II (two narrow overlap bands per monomer length); (c) FLS IV (one broad overlap band per monomer length); (d) FLS III (four narrow overlap bands per monomer length).

provided much of the current insight on the ultrastructure of collagen fibrils. The generally accepted Hodge–Petruska model (Petruska and Hodge, 1964), which describes the axial arrangement of collagen molecules in the native fibril, has its basis in TEM micrographs of negatively stained samples. As a tool for visualization, the AFM can serve as an excellent complementary approach to EM, and in a number of polymer studies, a combination of both AFM and TEM have been used to successfully obtain structural information (Goh, 1995). The first question to consider is the correlation of information from both techniques, which may not be a simple task because of their intrinsically different contrast mechanisms. The AFM attains contrast primarily from surface topography, whereas in negatively stained TEM images, contrast is generated by preferential exclusion or adsorption of heavy metal ions into the sample. In the

following, we will correlate AFM and TEM images for the case of FLS fibrils.

As noted in the introduction, FLS fibrils refer to a class of collagen fibrils with axial periodicity greater than the 60–70 nm of native-type collagen (Ghadially, 1988). Chapman and Armitage (1972) have classified these forms into four types based on the differences in their TEM banding patterns. These variants are shown schematically in Fig. 2 and in electron micrograph form in Fig. 7a–d (reprinted with permission of the publisher). The micrographs were generated by negative contrast staining with a sodium phosphotungstate solution, and thus the observed periodicity of FLS is due to a pattern of light-coloured bands, which are rich in electron-transmitting material, separated by broad dark bands, which are localized electron-opaque material. The dark regions in TEM micrographs are generally believed to correspond to stain-penetrable, less densely packed regions of the fibril; in normal collagen, these are the so-called 'gap-zones' of the Hodge–Petruska model. A more careful consideration also takes into account an enhanced uptake of ions into polar regions of molecules, as well as stain exclusion by bulky amino acid groups (Chapman et al., 1990).

In our AFM studies of FLS fibrils, we see two types that can be differentiated by their banding patterns, which we label Type A and Type B. It is not immediately obvious which of the various classifications assigned by Chapman and Armitage (e.g. FLS I–FLS IV), if any, correspond to these. We shall propose that Type A corresponds to FLS I and Type B to FLS IV based on the arguments below.

In the TEM images of collagen, one typically observes broad gap/overlap zones, with small scale variations in the stain patterns in these regions. The nature of these small-scale variations have been studied in detail and are well understood (Chapman et al., 1990). Let us, however, consider the collagen fibril staining process itself. In this process, a solution of sodium phosphotungstate is directly applied to the sample, and allowed to interact for a few seconds. Note that the approximate size of a phosphotungstate polyanion is of the order of 1 nm (Keggin, 1934; Chapman et al., 1990). In order to settle into crevices buried within the fibrils, this anion will have to penetrate the surface of the fibril. The surface topography of the fibril is easily visualized with the AFM, and we can use the AFM images to provide guidance in estimating possible stain penetration into the fibril. In mature FLS fibrils, such as that shown in Fig. 4a, we observed a tight packing of protofibrils. Given the spacing between protofibrils (groove depth ~2 nm, width 20–25 nm), it is highly unlikely that the stain can penetrate into the fibril to much more than a small fraction of its total diameter. This would mean that if there are gap zones in the fibril's interior, they cannot be easily reached by stain molecules, because the stain is too large to penetrate into the fibril to any significant degree. Instead, we propose that the contrast is mostly due to the behaviour of the stain at the surface of the fibrils.

Consider, instead, the deposition pattern of the stain on the surface of the fibril itself. Notice that the topographical section along the length of an FLS fibril (in Fig. 4b) shows that the banding pattern is due to alternating peaks ('bands') and valleys ('interbands'). The valleys are thus crevices between the peaks, and as the solution deposits the phosphotungstate stain, the crevices will be filled preferentially over the peaks. The net density of high electron scattering material in these interband regions will thus be much greater than on the bands themselves, making these regions appear dark in TEM. Thus, in this view, the dark bands in TEM, which indicate a high amount of deposited metal stain, will correspond to topographical crevices and valleys observed in the AFM, while the light bands in TEM will correspond to higher regions in the AFM images.

With these arguments in mind, we can attempt to correlate the different structural variants of collagen we have measured with the AFM to the corresponding TEM classifications. We shall generally assume that the light bands in TEM micrographs correspond to elevated topographical regions, and the dark bands correspond to 'low lying' regions in which the metal stain can collect. The Type A FLS we observed corresponds most closely to Chapman and Armitage's FLS I: From the TEM micrographs, the periodicity is caused by single bands separated by approximately 260 nm, with a band width of ~60 nm. The AFM images yield a comparable periodicity, and band widths of ~90–100 nm, with this latter value greater than the width measured by TEM because of the aforementioned AFM tip convolution effect. An examination of FLS IV shows that the periodicity in the TEM micrographs is caused by broad, light-coloured bands, separated by 260 nm, with the bands having an estimated width of ~150 nm. This is comparable with the Type B fibrils observed in our AFM work: the periodicity is the same and the band widths are ~200 nm. Again, accounting for tip convolution effects in the measured band widths, these are values which compare well with those for FLS IV.

3.4. Insights into assembly mechanism of FLS collagen

We have collected numerous images that have provided us with insight, albeit incomplete, into the mechanism by which FLS fibrils form. In our previous report (Paige et al., 1998), we noted the presence of protofibrils, stable intermediates in the assembly of FLS, with lengths of several microns and diameters of 5–7 nm. As mentioned above, the grooves observed along the length of the fibril are actually due to the spaces between adjacent protofibrils. These protofibrils bulge outwards at each band, but appear as continuous structures along the length of the fibril. We also observed these protofibrils adding to the end of a mature FLS fibril, suggesting that, at least in the later stages of assembly, FLS fibril growth occurs via the interweaving of protofibrils at the ends of fibrils. In order to elucidate the assembly mechanism, it would be most desirable if

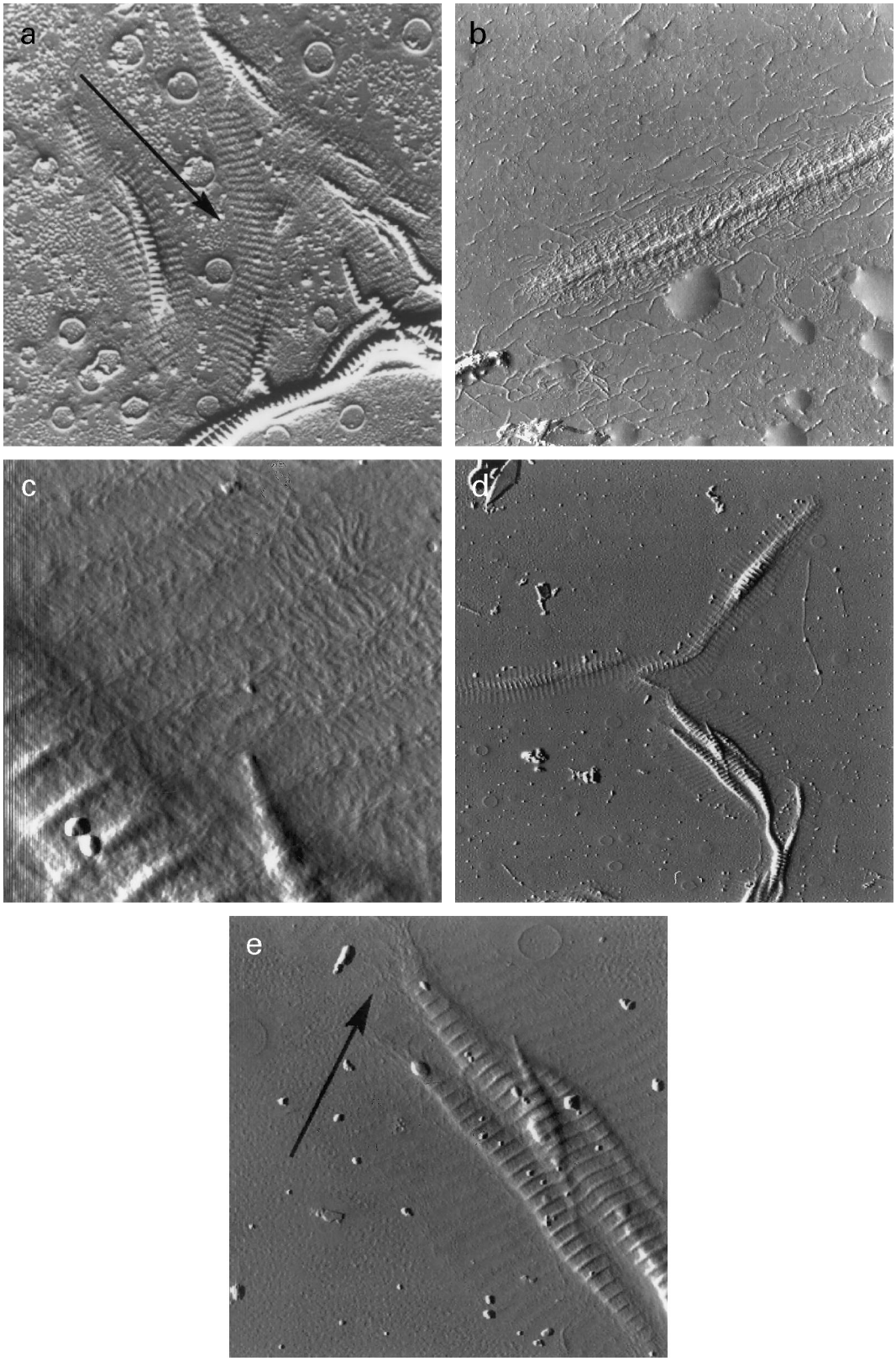

Fig. 8. AFM images of intermediate stages in FLS collagen assembly (deflection mode). (a) Network of interwoven collagenous material. Sectional analysis shows this material consists of collagen monomers or oligomers but not protofibrils. The network has a periodicity approaching the 250 nm of FLS collagen, yet no fibrillar structure has formed (25×25 μm). (b) Interwoven network of collagenous material showing an internal structure connecting it together (10×10 μm^2). (c) Zoom in of aligned collagenous material (2×2 μm^2). (d) FLS fibril with surrounding collagenous network (25×25 μm^2). (e) FLS fibril with protofibrils adding to its tip end (8×8 μm^2).

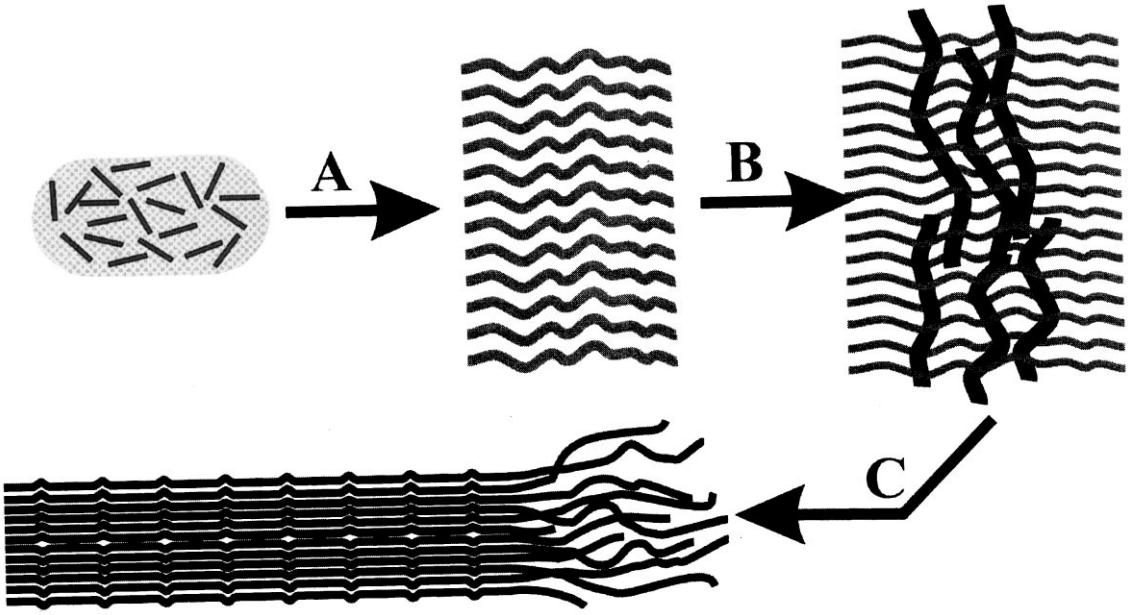

Fig. 9. Schematic illustration of postulated FLS assembly mechanism. Collagen monomers aggregate (step A) to form a framework of collagenous scaffolding material at the periodicity of banding (~250 nm) for the mature fibril. Protofibril structures begin interweaving (step B) with the framework, beginning to form bulk along the long axis of the fibril. As the fibril matures (step C), the scaffolding materials are incorporated into the fibril as it tightens and the protofibrils pack in a more orderly fashion. Growth continues via protofibrillar addition at the tips of the fibril.

one can observe fibrillogenesis as it takes place. However, technical difficulties have precluded us from performing such studies. Instead, we examined a large range of samples to provide information about the mechanism by which FLS forms. In Fig. 8a–e, we show a series of AFM images that were taken from samples prepared in the manner described above. The structures observed in these images coexist with one-another as well as with mature FLS fibrils within the same sample; however, the mature fibrils are the dominant forms, which is why they were more readily observed.

In Fig. 8a, we observe a periodic framework of collagenous material, which appears to be aligned in a lateral fashion. The spacing between these structures is ~300 nm, somewhat larger but close to the expected periodicity of FLS. These structures are stable in the absence of any resolvable fibrillar structure. In Fig. 8b, we observe a similar pattern of laterally aligned collagenous material, but with the beginning of an internal structure forming between them, something that hints to the subsequent appearance of a fibril. The banding pattern in this structure is easily discerned, and corresponds to the characteristic 260 nm of FLS. In Fig. 8c, we have zoomed in on the aligned, fibrous collagen material in one of these structures. This material has smaller dimensions than the protofibrils we have characterized previously: The diameters are of the order of ~1–2 nm, whereas the previously observed protofibrils had diameters from 5 to 7 nm. Whether these fibrous structures are purely oligomeric or contain monomers is unclear, as their high degree of entanglement and their tendency to pile on top of each other make any exact classification problematic. Fig. 8d shows a further development of this stage, again with the aligned collagenous material still being plainly obvious but with a much larger, banded internal structure connecting the periodic bands together. At this stage, the internal structure has a diameter of 20–30 nm, indicating that a great deal more lateral growth is required before it reaches the size of a typical mature FLS fibril (~150 nm diameter). Finally, in Fig. 8e, we show a blunted fibril end, with one end of the fibril showing the typical FLS banding pattern and the other showing protofibrils merging with the growing tip.

Because of the recurrence of images such as these, we suggest that FLS may grow in the following manner, which is schematically illustrated in Fig. 9. An initial framework consisting of entangled collagen monomers and oligomers aligns in solution, with the periodic arrangement being determined either by long-range interparticle forces, or by a thin network of collagen linkers that are smaller than the resolution attained in our experiments (Step A in Fig. 9). Concurrent to this interweaving of monomers and oligomers is the growth of protofibrils, a process likely competitive with the formation of the interwoven collagen framework. While maintaining the collagenous framework, monomers and oligomers add laterally, parallel to the long axis of the fibril, resulting in the gradual thickening of the FLS fibril (Step B in Fig. 9). Again, occurring simultaneously, is the addition of protofibrils to the end of the fibrils (segments of protofibrils are represented in Step B in Fig. 9). This results in structures that have the characteristic FLS banding pattern, but not the thickness of the mature fibrils. Simultaneous lateral growth, via addition of monomers and oligomers, as well as growth through the fibril tip end proceeds

until, at some point in the assembly, lateral growth ceases and growth of the fibril becomes dominated by addition of protofibrils to its tip (Step C in Fig. 9). This may occur because the supply of free monomers and oligomers in solution becomes exhausted, making protofibrils the only species able to add to the growing fibril. As protofibrillar addition progresses, the fibril is drawn together more tightly until the final, banded structure is formed. At some point in the assembly, addition of collagen between protofibrils ceases and the growth of the fibril becomes dominated by addition of protofibrils to its tip end. As addition progresses, the fibril is drawn together increasingly tightly, until the final structure is formed.

This model is, of course, speculative, and there are several issues that need to be addressed. The first is one of sample preparation. In the methods used here, samples are dried onto the mica substrate. Drying samples can induce unusual patterns in the material being deposited. In some cases, these drying patterns can be distinguished by an experienced microscopist. A common example of this would be the formation of circular patches, caused by the gradual evaporation of droplets on the surface. Other patterns can be less easy to recognize, raising the possibility that some of the results we have observed here may be a consequence of sample drying. However, we believe that this is not the case. If the patterns we observed were caused by drying, one would expect that the samples would orient themselves along the drying front; that is, all the fibrils, protofibrils and partially formed fibrils with their associated collagenous material would all be aligned in the same direction. This is definitely not the case in our experiments: For example, in Fig. 8d, the partially formed fibrils have a random orientation with respect to one another.

Another issue that should be addressed is one of kinetics. We have assumed that the diverse structures imaged represent different stages of the assembly process. Ideally, one would like to carry out a kinetic investigation, in which the appearance and development of these different structures is tracked as a function of time. However, this has not been possible so far. When samples are taken prior to completion of the dialysis, the collagenous material coagulates and cannot be dispersed on the mica substrate. Thus, they generally appear as amorphous clumps in the AFM images, preventing us from obtaining a better resolution. We are making further attempts at preventing this coagulation, or at least dispersing the clumps, in order to better characterize the time dependence of the fibril formation.

3.5. A possible explanation for FLS fibril banding

As discussed in the introduction, previous explanations for the banding patterns observed in FLS collagen have been based upon various staggering patterns of monomers. However, the protofibrillar make-up of mature FLS fibrils is inconsistent with this kind of model. The presence of protofibrils, and other collagenous intermediates, adds another level of complexity to the hierarchy of FLS assembly. In fact, no evidence whatsoever of monomer alignment in the production of the observed banding appears during AFM analysis.

The presence of a scaffolding of collagenous material demarcating the banding periodicity of the fibril long before the fibril itself is seen leads to an interesting hypothesis for the presence of bands in the mature FLS fibril. This scaffolding material appears to somehow promote the gathering and interweaving of protofibrils. As the fibril matures, the scaffolding material is not discarded, but incorporated into the growing fibril. Therefore, the bulges that are observed in FLS collagen, causing its highly periodic long-spacing band pattern, may in fact be caused by the incorporation of these apparent promoters of fibril formation.

It is important to note that the role of the α_1-acid glycoprotein in the apparent hierarchy of FLS assembly is still entirely unknown. Whether it is involved in the formation of the scaffolding, of the protofibrils, or of both cannot yet be discerned. This is an important factor that must be investigated further, especially if any understanding of FLS collagen assembly in vivo is to be obtained.

4. Summary

The ultrastructure of fibrous long spacing collagen has been examined by the atomic force microscope. We have noted the existence of two structural variants of FLS fibrils, the major difference between the structures being the presence of ridges adjacent to the central banding peak. The structures observed have been compared with those obtained from electron microscopy, and, taking into account the role of AFM tip convolution on the structure, the fibrils have tentatively been classified as FLS I and IV, as assigned by Chapman and Armitage in earlier TEM experiments. In addition, a series of images which show different stages of assembly of FLS have led us to speculate on possible mechanisms of fibril formation. Our proposed model involves the establishment of a preliminary framework of interwoven oligomers and monomers, followed by growth of the fibril around this framework and a final addition of protofibrils to the fibril tip ends. Furthermore, the periodicity of FLS fibril banding may in fact be attributable to the incorporation of this primary collagenous framework into the fibril during assembly.

References

Baselt, D.R., Revel, J.-P., Baldeschwieler, J.D., 1993. Subfibrillar structure of type I collagen observed by atomic force microscopy. Biophys. J. 65, 2644–2655.

Binnig, G., Quate, C.F., Gerber, C., 1986. Atomic force microscope. Phys. Rev. Lett. 56, 930–933.

Bustamante, C., Rivetti, C., Keller, D., 1997. Scanning force microscopy under aqueous solutions. Curr. Opin. Struct. Biol. 7, 709–716.

Cauna, N., Ross, L.L., 1960. The fine structure of Meissner's touch corpuscles of human fingers. J. Biophys. Biochem. Cytol. 8, 467–482.

Chapman, J.A., Armitage, P.M., 1972. An analysis of fibrous long spacing forms of collagen. Conn. Tiss. Res. 1, 31–37.

Chapman, J.A., Tzaphlidou, M., Meek, K.M., Kadler, K.E., 1990. The collagen fibril—a model system for studying the staining and fixation of a protein. Electron. Microsc. Rev. 3, 143–182.

Chicon, R., Ortuno, M., Abellan, J., 1987. An algorithm for surface reconstruction in scanning tunneling microscopy. Surf. Sci. 181, 107–111.

Dingemans, K.P., Teeling, P., 1994. Long-spacing collagen and proteoglycans in pathologic tissues. Ultrastruct. Pathol. 18, 539–547.

Dürig, U., Pohl, D.W., Rohner, F., 1986. Near-field optical-scanning microscopy. J. Appl. Phys. 59, 3318–3327.

Franzblau, C., Schmid, K., Faris, B., Beldekas, J., Garvin, P., Kagan, H.M., Baum, B.J., 1976. The interaction of collagen with alpha1-acid glycoprotein. Biochim. Biophys. Acta 427, 302–314.

Ghadially, F.N., 1988. Ultrastructural Pathology of the Cell and Matrix, Butterworths, London.

Ghadially, F.N., Mierau, G.W., 1985. An unusual banded structure in Ewing's sarcoma. J. Submicrosc. Cytol. 17, 645–650.

Goh, M.C., 1995. Atomic force microscopy of polymer films. Adv. Chem. Phys. 91, 1–83.

Gross, J., Highberger, J.H., Schmitt, F.O., 1952. Some factors involved in the fibrogenesis of collagen in vitro. Proc. Soc. Exp. Biol. Med. 80, 462–465.

Gross, J., Highberger, J.H., Schmitt, F.O., 1954. Collagen structures considered as states of aggregation of a kinetic unit. The tropocollagen particle. Proc. Natl Acad. Sci. USA 40, 679–688.

Hansma, H.G., Kim, K.J., Laney, D.E., Garcia, R.A., Argaman, M., Allen, M.J., Parsons, S.M., 1997. Properties of biomolecules measured from atomic force microscope images: a review. J. Struct. Biol. 119, 99–108.

Hashimoto, K., Ohyama, H., 1974. Cross-banded filamentous aggregation in the human dermis. J. Invest. Dermatol. 62, 106–112.

Highberger, J.F., Gross, J., Schmitt, F.O., 1950. Electron microscope observations of certain fibrous structures obtained form connective tissue extracts. J. Am. Chem. Soc. 72, 3321–3322.

Highberger, J.H., Gross, J., Schmitt, F.O., 1951. The interaction of mucoprotein with soluble collagen; an electron microscope study. Proc. Natl Acad. Sci. USA 37, 286–291.

Jakus, M.A., 1956. Studies on the cornea. II. The fine structure of Descemet's membrane. J. Biophys. Biochem. Cytol. 2, 243–255.

Kajikawa, K., Nakanishi, I., Yamamura, T., 1980. The effect of collagenase on the formation of fibrous long spacing collagen aggregates. Lab. Invest. 43, 410–417.

Kamiyama, R., 1982. Fibrous long spacing-like fibers in the bone marrow of myloproliferative disorder. Virchows Arch. B Cell. Pathol. Incl. Mol. Pathol. 39, 285–291.

Kamiyama, R., Shimamine, T., 1977. Fibrous long spacing-like fibers in the bone marrow of primary myelofibrosis. J. Electron. Microsc. 26, 339–341.

Keggin, J.F., 1934. The structure and formula of 12-phosphotungstic acid. Proc. R Soc. Lond. A 144, 75–100.

Keller, D., 1991. Reconstruction of STM and AFM images distorted by finite-size tips. Surf. Sci. 253, 353–364.

Kobayasi, T., Asboe-Hansen, G., Tsurufuji, S., 1985. Filamentous aggregates of collagen. Ultrastructural evidence for collagen-fibril degradation in situ. Arch. Dermatol. Res. 277, 214–219.

Lewis, A., Radko, A., Ben Ami, N., Palanker, D., Lieberman, K., 1999. Near-field scanning optical microscopy in cell biology. Trends Cell. Biol. 9, 70–73.

Lowther, D.A., Toole, B.P., Herrington, A.C., 1970. Interaction of proteoglycans with tropocollagen. In: Balazs, E.A. (Ed.). Chemistry and Molecular Biology of the Intercellular Matrix, Academic Press, New York, pp. 1135–1153.

Luse, S.A., 1960. Electron microscopic studies of brain tumors. Neurology 10, 881–905.

Markiewicz, P., Goh, M.C., 1994. Atomic-force microscopy probe tip visualization and improvement of images using a simple deconvolution procedure. Langmuir 10, 5–7.

Markiewicz, P., Goh, M.C., 1997. Identifying locations on a substrate for the repeated positioning of AFM samples. Ultramicroscopy 68, 215–221.

Meixner, A.J., Kneppe, H., 1998. Scanning near-field optical microscopy in cell biology and microbiology. Cell. Mol. Biol. (Noisy-le-grand) 44, 673–688.

Miki, H., Unno, K., Park, P., Ohno, T., Nakajima, M., 1993. Morphogenesis and origin of fibrous long-spacing collagen fibers in collagenase-treated mouse skin tissues. Tissue Cell. 25, 669–680.

Morris, C.J., Bradby, G.V., Walton, K.W., 1978. Fibrous long-spacing collagen in human atherosclerosis. Atherosclerosis 31, 345–354.

Nakanishi, I., Masuda, S., Kitamura, T., Moriizumi, T., Kajikawa, K., 1981. Distribution of fibrous long-spacing fibers in normal and pathological lymph nodes. Acta Pathol. Jpn 31, 733–745.

Naumann, R.A., Wolfe, D.E., 1963. A striated intercellular material in rat brain. Nature 198, 701–703.

Nimni, M.E., 1988. Collagen, CRC Press, Boca Raton, FL.

Paige, M.F., Rainey, J.K., Goh, M.C., 1998. Fibrous long spacing collagen ultrastructure elucidated by atomic force microscopy. Biophys. J. 74, 3211–3216.

Park, P., Ohno, T., 1985. Ultrastructural study of long spacing collagen fibres and basal lamina in malignant schwannoma. Tissue Cell. 17, 699–707.

Petruska, J.A., Hodge, A.J., 1964. A subunit model for the tropocollagen macromolecule. Proc. Natl Acad. Sci. USA 51, 871.

Revenko, I., Sommer, F., Minh, D.T., Garrone, R., Franc, J.M., 1994. Atomic force microscopy study of the collagen fibre structure. Biol. Cell. 80, 67–69.

Sarid, D., 1991. Scanning Force Microscopy with Applications to Electric, Magnetic and Atomic Forces, Oxford University Press, Oxford.

Shao, Z., Zhang, Y., 1996. Biological cryo atomic force microscopy: a brief review. Ultramicroscopy 66, 141–152.

Shiku, H., Dunn, R.C., 1999. Near-field scanning optical microscopy. Anal. Chem. 71, 23A–29A.

Slavin, R.E., Swedo, J.L., Brandes, D., Gonzalez-Vitale, J.C., Osornio-Vargas, A., 1985. Extrapulmonary silicosis: a clinical, morphologic, and ultrastructural study. Hum. Pathol. 16, 393–412.

Williams, B.R., Gelman, R.A., Poppke, D.C., Piez, K.A., 1978. Collagen fibril formation. Optimal in vitro conditions and preliminary kinetic results. J. Biol. Chem. 253, 6578–6585.